Title

Digitally controlled simple shear apparatus for dynamic soil testing

Permalink

https://escholarship.org/uc/item/1vg0k9xs

Journal

Geotechnical Testing Journal, 30(5)

Authors

Duku, Pendo M
Stewart, Jonathan P
Whang, Daniel H
et al.

Publication Date

2007

Peer reviewed

P. M. Duku,[1] J. P. Stewart,[1] D. H. Whang,[2] and R. Venugopal[3]

Digitally Controlled Simple Shear Apparatus for Dynamic Soil Testing*

ABSTRACT: We describe the characteristics of a simple shear apparatus capable of applying realistic multidirectional earthquake loading to soil specimens. This device, herein termed the Digitally Controlled Simple Shear (DC-SS) apparatus, incorporates features such as servohydraulic actuation and true digital control to overcome control limitations of some previous dynamic soil testing machines. The device is shown to be capable of reproducing sinusoidal and broadband command signals across a wide range of frequencies and amplitudes, although the device has limited control capabilities for very small command displacements (less than approximately 0.005 mm). The small deformation limitation results from noise introduced to the control system from analog-to-digital conversion of feedback signals. We demonstrate that bidirectional command signals can be accurately imparted with minimal cross coupling, which results from an innovative multiple-input, multiple-output digital control system. The capabilities of the device are demonstrated with a series of broadband tests on unsaturated soil specimens subjected to uni- and bidirectional excitation.

KEYWORDS: digital control, simple shear, dynamic soil testing, multidirectional loading

Introduction

Direct simple shear apparatuses have been utilized successfully for many years to characterize static and dynamic soil properties. This method of testing is often preferred when it is desirable for the specimen to experience a smooth and continuous rotation of the principal stress directions during shear. Initial stresses can be applied to simulate at-rest field conditions when wire reinforced membranes are utilized that minimize lateral distortion of the sample (i.e., the NGI-type configuration, Bjerrum and Landva 1966). Perhaps the most common application of simple shear testing has been for the simulation of vertical (or nearly vertical) shear wave propagation through a soil column. Advantages and limitations of simple shear tests relative to other types of laboratory tests have been described elsewhere and are not repeated here (e.g., Lucks et al. 1972; Shen et al. 1978; Saada et al. 1982; Vucetic and Lacasse 1982; Budhu 1985; Bhatia et al. 1985; Amer et al. 1987; Airey and Wood 1987; Budhu and Britto 1987; Boulanger et al. 1993).

Most simple shear apparatuses operate in a single horizontal direction and apply harmonic loading at frequencies which are typically slower than dynamic processes such as earthquake shaking (e.g., Tatsuoka and Silver 1981; Doroudian and Vucetic 1995; Lefebvre and Pfender 1996; Riemer and Seed 1997; Kusakabe et al. 1999; Hazirbaba and Rathje 2004). While there are always approximations involved in applying soil properties measured in the laboratory to field conditions, the inability of existing devices to provide rapid, multidirectional loading introduces further errors of unknown significance when laboratory-measured soil properties are used in engineering simulations.

A number of simple shear apparatuses have been developed to investigate soil response to multidirectional loading (e.g., Ishihara and Yamazaki 1980; Boulanger et al. 1993; DeGroot et al. 1996). The University of California, Berkeley bidirectional cyclic simple shear (UCB-2D) device is noteworthy since it significantly reduced mechanical compliance issues that caused relative top/base cap rocking in earlier devices (e.g., Ishihara and Yamazaki 1980; Ishihara and Nagase 1988). Another significant feature of the UCB-2D device is chamber pressure control, which facilitates back pressure saturation.

The principal limitation of the UCB-2D device, and earlier devices, is their inability to apply earthquake-like broadband loading at rapid displacement rates. This limitation also exists for most unidirectional simple shear devices. The reasons for this are twofold: (1) pneumatic loading systems use a compressible fluid (i.e., air) which introduces significant errors to the feedback loop at high frequencies; and (2) digitally-supervised analog controllers were employed which effectively limit the processing speed and sophistication of the control algorithms. Of course, shaking table and centrifuge experiments are capable of applying multidirectional earthquake-like loading to soil models (i.e., Pyke et al. 1975; Jafarzadeh and Yanagisawa 1998; Kutter 1995; Wilson et al. 2004). However, direct measurements of the soil element response (e.g., shear stress-shear strain relationships, volumetric strain, and pore water pressure) in these types of experiments requires dense instrumentation arrays that can affect the response they are intended to measure, which in turn complicates data interpretation (e.g., Elgamal et al. 2005).

The capability of applying, with a reliable degree of control, multidirectional loading across a wide range of frequencies to soil elements in the laboratory is critical to advancing our fundamental understanding of dynamic soil properties. For example, broadband loading capabilities are needed to investigate rate effects on soil

[1] Graduate Student Researcher and Associate Professor and Vice Chair, respectively, Department of Civil & Environmental Engineering, University of California, Los Angeles, 5731 Boelter Hall, Los Angeles, CA 90095.

[2] Engineer, Exponent Failure Analysis, 320 Goddard, Suite 200, Irvine, CA 92618.

[3] Founder and Senior Consulting Engineer, Sysendes, Inc., 1804 Tupper, Suite 4, Montréal, QC H3H 1N4, Canada.

*The views and conclusions contained in this document are those of the authors and should not be interpreted as necessarily representing the official policies, either expressed or implied, of the U.S. Government.
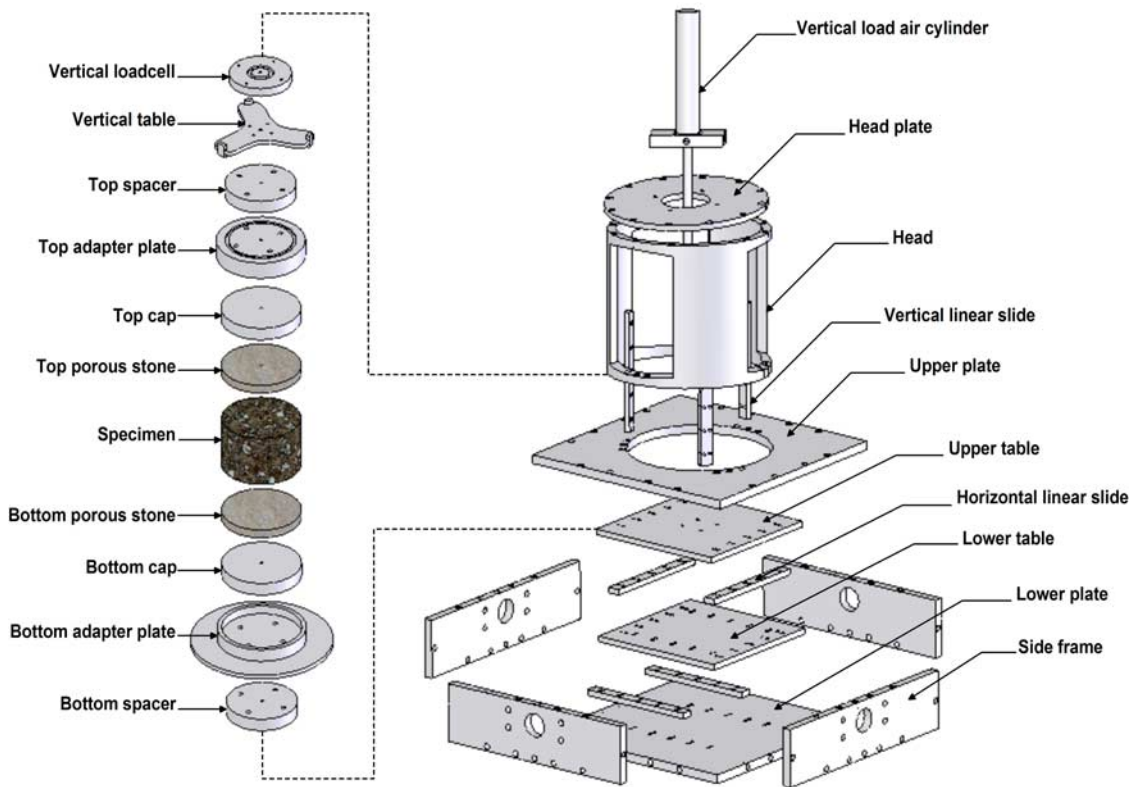
FIG. 1—*Schematic of the DC-SS device at UCLA.*

properties, which are known to be significant for clays (e.g., Lefebvre and Pfender 1996; Sheahan et al. 1996). Moreover, the effect of shear rate and 2D loading on pore pressure generation or volume change behavior, or both, is less well understood and requires further investigation for some soil types. To meet these research needs, a digitally-controlled simple shear device with capabilities for chamber pressure control and multidirectional excitation has been developed. This device, herein termed the <u>D</u>igitally-<u>C</u>ontrolled <u>S</u>imple <u>S</u>hear (DC-SS) apparatus incorporates features such as servohydraulic actuation and true digital control to overcome the limitations of previous dynamic soil testing machines. The result is a truly unique simple shear apparatus with the capability to apply broadband (earthquake-like) displacement demands on soil specimens in two directions and with minimal cross coupling between the horizontal motions. In this paper, we describe this device and its capabilities for dynamic soil testing.

Physical Description of DC-SS Device

The mechanical design of the DC-SS device was developed using the UCB-2D device as a prototype (Boulanger et al. 1993). The DC-SS device was designed to retain the main features of the UCB-2D device such as inclusion of cell pressure for purposes of back pressure saturation, limited mechanical compliance with respect to simple shear boundary conditions (e.g., top and base platen "rocking"), and bidirectional loading capability. In addition to these features, the DC-SS device incorporates several design improvements relative to the UCB-2D device including: (*i*) the use of a tri-post frame with high performance track bearings (which accommodate vertical displacements of the top cap) to further reduce

rocking; (*ii*) a servohydraulic control system to allow for high frequency loading; and (*iii*) a dual axis load cell to obtain post-friction shear load measurements.

Figure 1 shows the general assembly of the DC-SS apparatus. Photographs of the DC-SS device are shown in Fig. 2. The DC-SS device was designed to test cylindrical soil specimens with a diameter of 10.2 cm or less. The specimen is located between relatively rigid bottom and top caps (Fig. 1, Fig. 2(*b*)) and is typically confined by a wire reinforced membrane. As shown in Fig. 2(*c*), the horizontal (top and bottom) faces of the specimen are confined by the caps, which contain fine porous stones epoxied into a recess covering the entire face of the cap except for a retaining lip of aluminum around the edge. These caps provide a "frictional" surface while allowing for drainage into the porous stones if the stones are unsaturated (the stones can be saturated for undrained tests). The top cap/specimen/bottom cap stack is positioned between the top and bottom adapter plates shown in Fig. 1. The bottom cap fits into a recess within the bottom adapter plate. The top adapter plate is gently lowered such that a recess within the top adapter plate fits snugly over the top cap. The top and bottom caps are held tightly on their respective adapter plates by three set screws on each plate. Once the specimen is secured between the two adapter plates, three LVDTs equally spaced around the specimen are mounted on the top adapter plate and fixed to the plate by set screws. The specimen is then consolidated by a vertical stress and is ready for shear loading.

Above the top adapter plate is a vertical table, which in turn is attached to a vertical load cell (Fig. 1). Vertical loads are transferred to the specimen through the vertical table, which is attached to three equally spaced linear slides. Each of the three linear slides is attached to a separate post, which effectively precludes lateral movements and rocking of the vertical table (and hence, practically
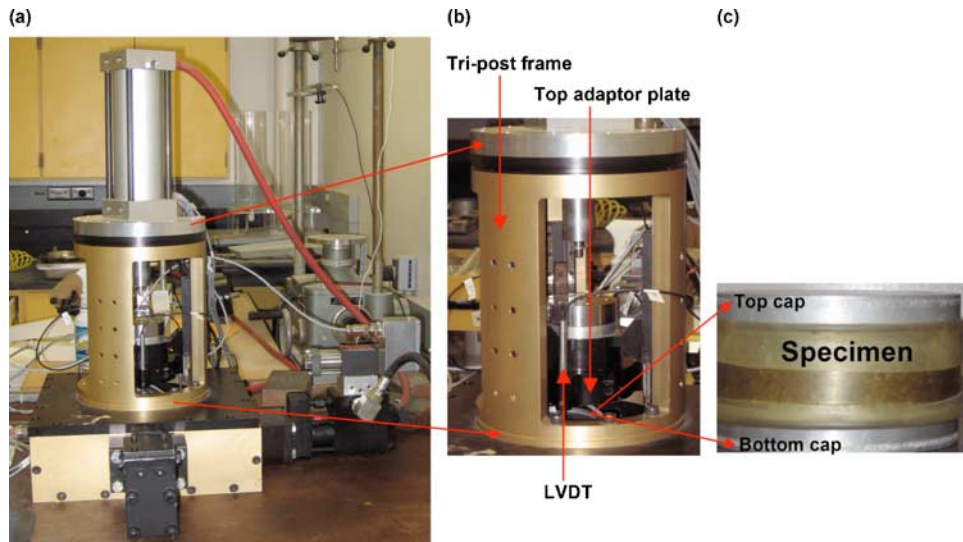
FIG. 2—*Photographs showing (a) overview of device, (b) close-up view of tri-post frame and top adapter plate, and (c) view of sample with top and bottom caps along with wire-reinforced membrane.*

speaking, the specimen as well). This tri-post frame is a significant improvement over the UCB-2D device, which employed a cantilever system (vertical table attached to a pair of track bearings along the same wall). Loads are applied to the vertical table by a pneumatic actuator mounted outside the main frame.

An important feature of the DC-SS device that was retained from the UCB-2D device is its bidirectional loading capability. Horizontal shear loads are applied at the base of the specimen through two independently controlled horizontal tables. The bottom horizontal table is mounted on linear slides attached to the main frame of the apparatus, and this table is free to move in only one horizontal direction. The upper horizontal table is also mounted on linear slides such that the movement of the upper table is exactly perpendicular to the lower table. The two horizontal tables can be controlled to produce net resultant movements of the bottom adapter plate in any horizontal direction. Loads are applied to the lower horizontal table by threaded rods that are attached to an actuator that can apply tension and compression. There is a tension-capable roller connection between the upper table and its actuator to accommodate perpendicular displacements of the lower table.

The loads applied to the tables are measured by loadcells mounted between the actuators and the tables. The loads measured by the loadcells are not identical to those imparted to the specimen due to friction in the linear slides. The magnitude of the frictional load within the system was characterized and observed to be quite small (approximately 2.2 N). The significance of this frictional load is dependent on what type of testing is desired. This frictional load will produce inaccuracies of approximately 0.3 kPa (for a 10.2-cm diameter specimen), which represents a negligible percentage of the shear stress for most applications. However, if very low stress measurements are needed, post-friction shear stresses can be measured by using a dual-axis loadcell. The dual-axis loadcell fits in between the top adapter plate and the vertical table, a space which is otherwise occupied by a spacer block. The dual-axis loadcell is capable of measuring both the vertical and shear loads simultaneously with minimal cross talk between these channels. However, the presence of the dual-axis loadcell introduces system compliance (i.e., rocking and vertical deformations) that may be significant at medium to large strains. Therefore, most tests are performed without the dual-axis loadcell in place.

Three LVDTs (linear variable differential transducers), mounted between the top and bottom adapter plates, are used to measure the vertical specimen deformations. These locations of LVDTs minimize errors due to mechanical compliance. The three LVDTs are used so that relative rocking of the specimen in either direction of loading can be measured. Data from the three LVDTs are averaged to define specimen height during a test. Horizontal deformations are measured by two LVDTs mounted to the horizontal tables in orthogonal directions.

The DC-SS device operates under "strain-control" conditions, meaning that table displacements are controlled and the actuator forces required to achieve those displacements are measured. The motions that can be imparted to the tables are limited by different aspects of the control system for different frequency bands. At low frequencies ($f \leq 0.24$ Hz), the limiting factor is the peak actuator displacement ($u_{max} = 51$ mm). At intermediate frequencies (0.24 Hz $< f \leq 15$ Hz), the limiting factor is the flow rate capacity of the servo-valve ($Q_{max} = 158$ cm^3/s). At frequencies $f > 15$ Hz, the limiting factor is the pressure capacity of the hydraulic pump ($p_{max} = 21$ MPa). For the case of harmonic control signals, these quantities can be related to the peak table motions as follows:

$$u(t) = D \sin(\omega t) \leq u_{\max} \tag{1}$$

$$\dot{u}(t) = D\omega \cos(\omega t) \leq Q_{\max}/A \tag{2}$$

$$\ddot{u}(t) = -D\omega^2 \sin(\omega t) \leq p_{\max}A/m \tag{3}$$

where $u(t)$ and its derivatives describe the table displacement, velocity, and acceleration, A is the cross-sectional area of the actuator (20.3 cm^2), m is the table mass (5.7 kg), and ω is the frequency of table motion (in radians/s). The corresponding peak values of displacement, velocity, and acceleration are given in Fig. 3. The control system is capable of producing any motion that lies below the limit lines in Fig. 3.

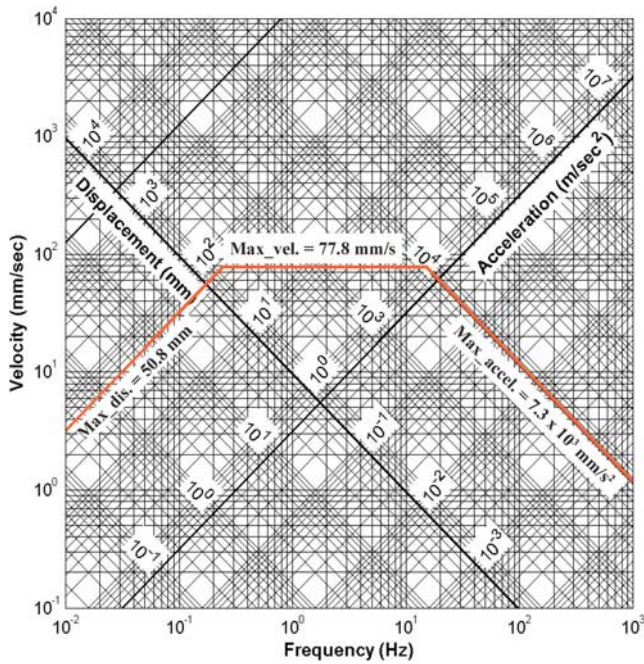The theoretical oil column frequency of the actuator-table system is given by Conte and Trombetti (2000):

FIG. 3—*Tripartite plot demonstrating the theoretical limitations of the DC-SS device.*

$$f_{oil} = \frac{A}{\pi} \sqrt{\left(\frac{\beta}{Vm}\right)} = 16.5 \text{ Hz} \qquad (4)$$

where β is the bulk modulus of the hydraulic fluid $(1.7 \times 10^6 \text{ kPa})$ and V is the volume of oil in the actuator (463 cm^3). Physically, the oil column frequency represents the natural frequency of the SDOF hydraulic actuator system, which can be visualized as the table mass connected to a spring having a stiffness that is defined by the oil column in the actuator chamber. For command signals with frequencies near the oil column frequency, the performance of the actuator can be limited due to resonance behavior (e.g., Conte and Trombetti 2000).

DC-SS Control System

As illustrated in Fig. 4, the digital control system for the DC-SS device serves two purposes. The first is to provide control signals to

direct drive servovalves that drive hydraulic actuators for each axis (direct drive servovalves have an onboard controller that corrects tracking errors in the control signal before driving the hydraulic actuators). The second purpose is to acquire data from the LVDTs and loadcells. The physical device referred to here as DC-SS was originally developed with a PC-based digitally-supervised analog control system. This control system used a PID (Proportional-Integral-Derivative) control algorithm that ran within a Windows™ operating system. The principal problem with that control system was latency in the processing of feedback signals from instruments (such as an LVDT) and the generation of command signals. This limited the ability of the device to accurately replicate some command signals. These problems were especially acute for loading functions involving fast velocities and 2D shaking. The system was successfully used in previous testing (e.g., Whang et al. 2004; Whang et al. 2005), although those applications involved unidirectional shaking and a 1.0 Hz loading frequency, so control problems associated with the PC-based system were not significant.

The control system for the present device uses a system referred to as hard real-time digital control. The principal difference from PC-based digital control is that the control functions are implemented on the controller board as opposed to a PC operating system. This enables guaranteed sampling frequencies for the internal feedback loop of 5 kHz using displacement feedback from the horizontal LVDTs, whereas PC-based digitally-supervised analog control systems typically cannot reliably execute the computations required for complex control at feedback sampling frequencies higher than 200 Hz, depending on the processor clock speed, control algorithm sophistication, number of background processes handled by the PC operating system, etc. The digital control system utilizes two dSPACE DS1104 controller boards. Each board contains a PowerPC 603e processor, four 16-bit 2 μs analog-to-digital (A/D) converters, four 12-bit 800 ns A/D converters and eight 16-bit 10 μs digital-to-analog (D/A) converters, in addition to other input/output ports. The two boards are mounted in PCI slots in a host PC but run their own real-time kernel (i.e., an operating system specifically tailored for control functions) independent of the host PC's operating system.

A PID control algorithm was implemented for both PC-based and hard real time digital control. This is referred to subsequently
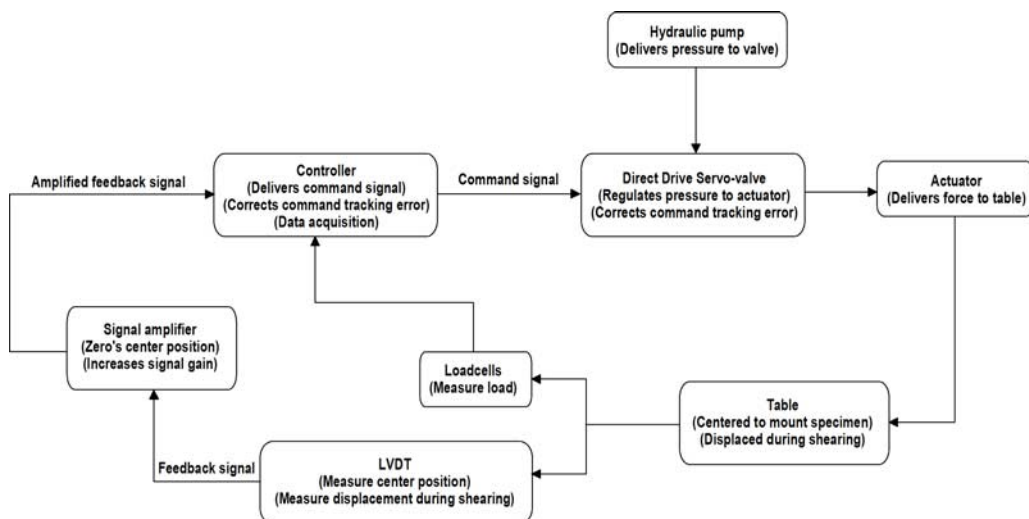

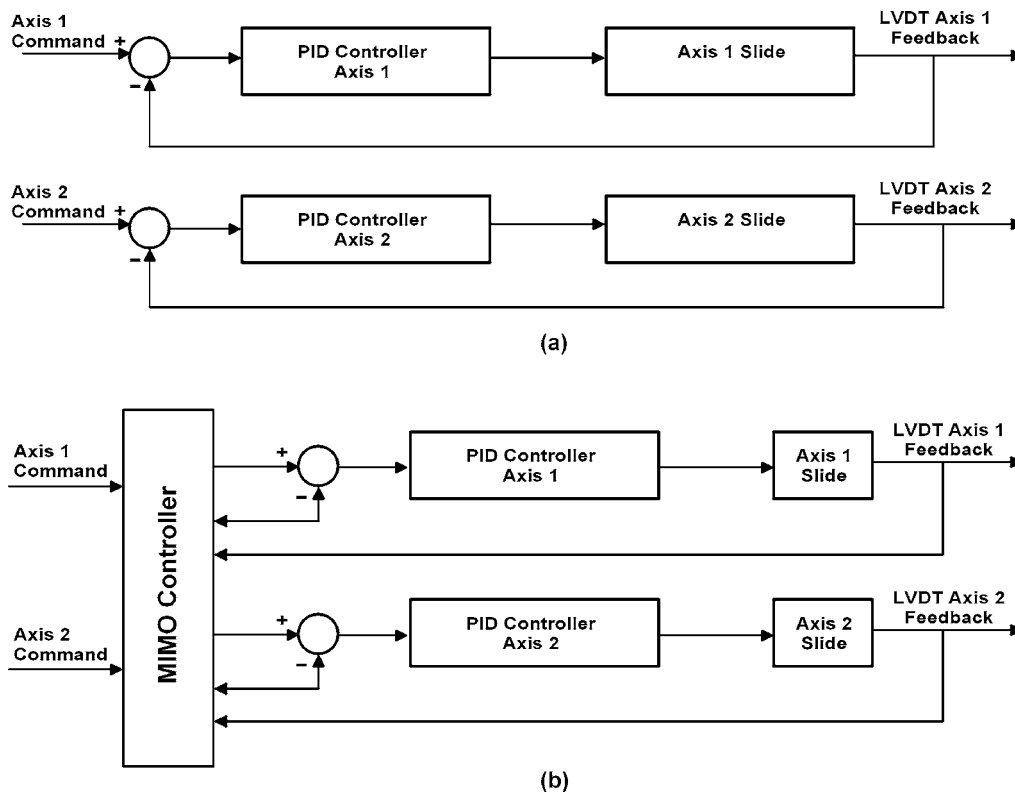FIG. 4—*Layout of the different elements of the DC-SS device.*

FIG. 5—*Controller architectures for (a) independent PID controller, and (b) MIMO-PID controller.*

as the "PID controller". Gains for the PID controller are tuned by trial-and-error for optimal performance using a step function command signal. The output of the PID controller is a digital voltage command that is sent to a Moog voltage amplifier via one of the D/A channels on the dSPACE board. The voltage amplifier, in turn, sends a voltage drive signal to the appropriate actuator servovalve. As illustrated in Fig. 5(*a*), PID control of the two axes are independent, and hence the control system as a whole is unable to compensate for cross-coupling effects (i.e., the influence of motion along one axis on the motion along the second axis).

In order to minimize cross-coupling effects, the digital control system was enhanced by introducing a multiple-input multiple-output (MIMO) control algorithm that interfaces with the PID controllers. As illustrated in Fig. 5(*b*), this controller uses LVDT feedback from both axes and generates a compensated command signal for each of the PID controllers, taking into account cross-coupling effects. The controller is designed and implemented as a discrete-time state space system using the LQG (Linear-Quadratic-Gaussian) optimal control method (Franklin et al. 1990). This method requires the estimation of four empirical quantities that reflect system properties. This is accomplished using the N4SID system identification algorithm (Van Overschee and De Moor 1995). System identification algorithms operate on input-output data sequences; the data used for this purpose were two uncorrelated random inputs (generated by the PID controllers) and the corresponding LVDT output signals.

The combination of the MIMO control algorithm and the two PID controllers is referred to subsequently as the "MIMO-PID" controller. The DC-SS device is configured so that the MIMO algorithm can be turned on or off. Hence, either PID or MIMO-PID digital control of experiments is possible. Data acquisition capabilities for either mode are summarized below:

- Input motion time step: no practical lower limit;
- Number of input motion data points: no practical upper limit;
- Feedback sampling frequency (i.e., the internal frequency for the feedback loop): 5 kHz;
- Data logging frequency: upper bound is 5 kHz, can be down-sampled as needed.

DC-SS System Performance

To evaluate the performance of the DC-SS system (i.e., controller, pump, actuators, and servo-valves), both harmonic and broadband earthquake input motions were specified to the PID controller and the MIMO-PID controller and the resulting feedback signals were measured. Unidirectional tests were performed to evaluate the performance of each axis independently, and to provide baseline results for evaluating interaction effects. Bidirectional loading was performed to evaluate cross-coupling between axes.

Sinusoidal Tracking

Figure 6 shows displacement histories and Fourier amplitude spectra of a displacement-controlled unidirectional harmonic command signal with amplitudes $u=0.20$ mm and 0.012 mm (corresponding to shear strain values of 1.0 and 0.06 %, respectively, for a typical 2-cm tall specimen) and $f=1$ Hz along with the feedback signals obtained using the MIMO-PID controller. The LVDT feedback signals were recorded using a sampling frequency of 200 Hz. The tests shown in Fig. 6 were performed in only one direction (zero command signal in the perpendicular direction).
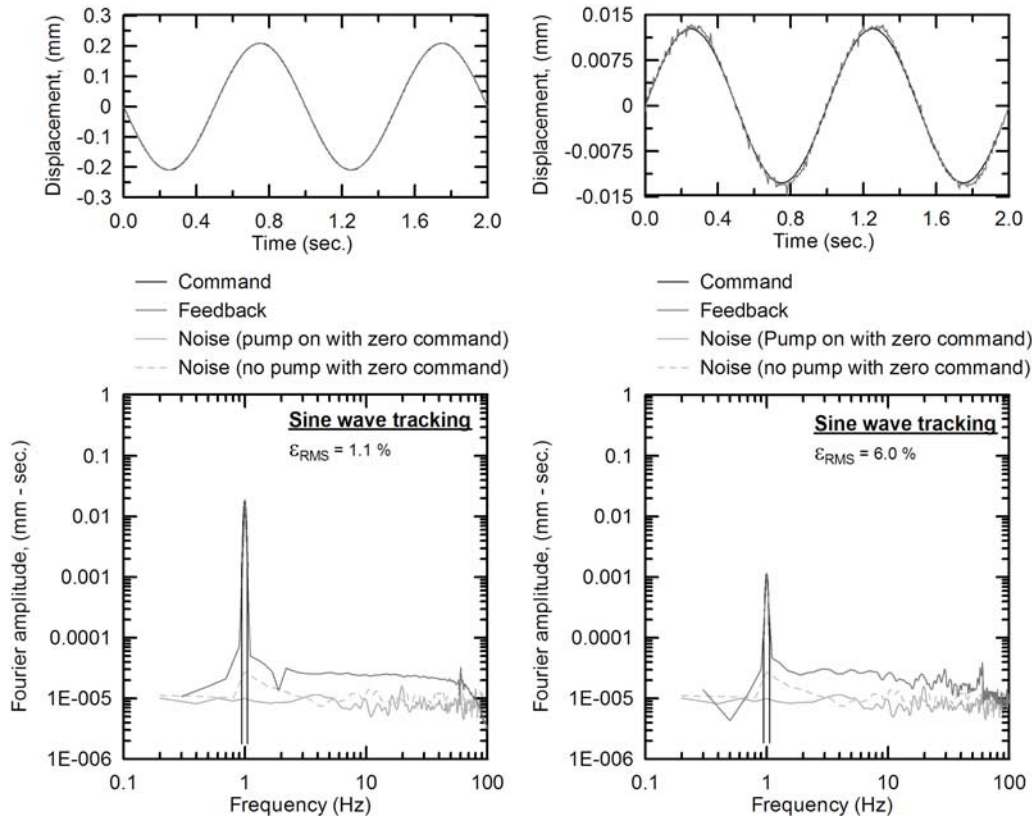
FIG. 6—*Sinusoid tracking of cyclic displacement amplitudes=0.2 and 0.01 mm at f=1 Hz for shearing along one axis at a time and noise level with pump on and off (MIMO controller).*

The upper plots in Fig. 6 show the feedback and command signals in the time domain. Visual inspection of the signals indicates better performance at larger amplitudes (u=0.20 mm). There is a time lag between the command and feedback of about 0.005 to 0.010 sec (one to two times the time step of 0.005 sec), which is consistently observed regardless of the loading frequency. This lag has been removed in the plots shown in Fig. 6 and subsequent plots. Following lag removal, the normalized root mean square error of the feedback signal is calculated as:

$$\text{Normalized RMS tracking error, } \varepsilon_{RMS} = \frac{\sum_{i=1}^{N} (x_i^c - x_i^f)^2}{\sum_{i=1}^{N} (x_i^c)^2} \quad (5)$$

where x^c denotes the command signal, x^f denotes the feedback signal, and the summation occurs over time (N is the number of time steps in the displacement histories). Values of ε_{RMS} for 1 Hz shaking were computed to be 1.1 and 6.0 % for u=0.20 mm and 0.01 mm, respectively.

The lower plots in Fig. 6 show the feedback and command signals in the frequency domain. Also shown for reference are noise spectra obtained with zero command signal and "pump on" and "pump off" conditions. The DC-SS device has one pump that operates the two valves (one on each horizontal axis). The no pump signal is electrical noise in the system and has a flat Fourier spectrum, which is consistent with white noise. System testing indicates that this noise is dominated by analog-to-digital (A/D) conversion of the feedback signal. This A/D noise is minimized by amplifying the feeback signal prior to the A/D conversion using the signal amplifier depicted in Fig. 4. In Fig. 6, the pump on spectrum essen-

tially matches the no pump spectrum, indicating that there is no perceptible actuator movement due to leakage of hydraulic oil through the spool in the valve while the pump is running. Note that the Fourier amplitude of the feedback signal matches that of the command signal at frequencies where the command signal is stronger than the noise spectrum, whereas outside of that relatively narrow frequency range, the spectra of the feedback signal is slightly stronger than the noise spectrum.

Figure 7 presents the variation of ε_{RMS} with harmonic loading frequency and displacement amplitude in unidirectional tests. As shown in Fig. 7(a), tracking errors for f=1 Hz were observed to decrease with increasing displacement for $u<0.2$ mm. This trend results from the increasing significance of system noise, illustrated in Fig. 6, as displacement amplitude decreases. The above results were obtained for unidirectional tests performed along Axis 1; practically identical results were obtained for Axis 2 that are not shown here for brevity. Figure 7(b) shows the effect of frequency for two displacement amplitudes (u=0.02 and 0.2 mm). In general, values of ε_{RMS} were observed to increase with increasing frequency.

Also shown in Fig. 7(a) are system errors for PID control relative to those for MIMO-PID control. As expected for unidirectional testing, error terms for both controllers are practically identical. Most of the tests reported in Fig. 7 were conducted with no sample and effectively zero normal stress acting on the sliding tables. To evaluate the effect of normal stress acting through a specimen, a separate test with the MIMO-PID controller was conducted with a specimen loaded to a normal stress of 101.3 kPa. The result, shown by the triangle in Fig. 7(a), indicates no noticeable effect on the ε_{RMS} values.
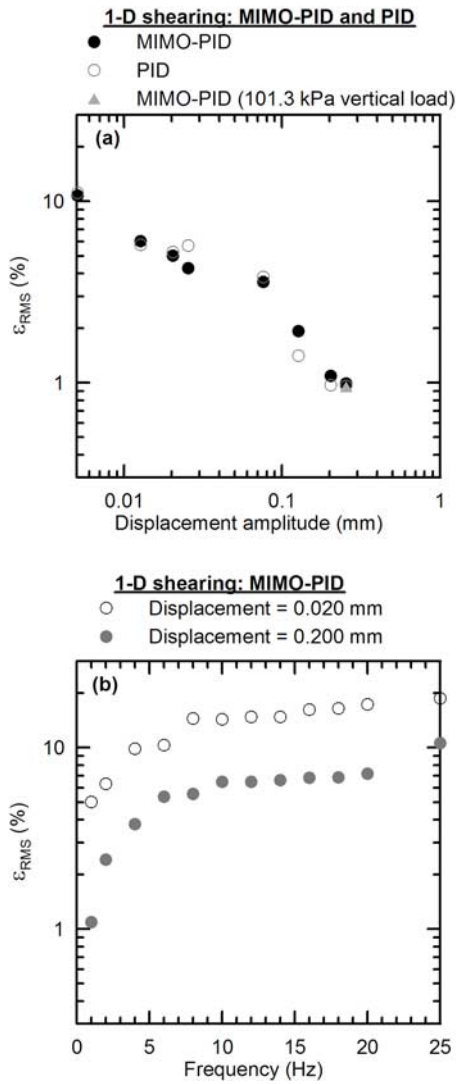
FIG. 7—*Variation of normalized root mean square of tracking errors for unidirectional shaking with (a) displacement amplitude, and (b) loading frequency. Note: for a typical 2-cm tall specimen, the displacement range in Part (a) corresponds to a strain range of 0.01 to 10 %.*

Interaction effects were investigated by providing simultaneous harmonic command signals in two horizontal directions. One axis is referred to as the baseline axis, and was consistently commanded a displacement amplitude of 0.20 mm at $f=1$ Hz frequency. The second axis was commanded simultaneously with a sinusoidal amplitude of 0.20 mm at $f=2, 4, 6, 8,$ and 10 Hz. Different frequencies were used for the second axis so that any cross-coupling effects could be readily identified (e.g., a significant feedback signal for the baseline axis at the excitation frequency for the second axis would indicate cross coupling). The results are summarized in Fig. 8 in the form of misfit of the baseline axis command/feedback signals as quantified by ε_{RMS}. In Fig. 8, results for zero frequency indicate no commanded motion of the perpendicular axis. The results in Fig. 8 illustrate two important points: (1) ε_{RMS} on the baseline axis is increased by the presence of shaking on the perpendicular axis but is not significantly affected by the frequency of shaking on the perpendicular axis (observed by comparing results at zero frequency with finite frequencies); (2) ε_{RMS} is lower for MIMO-PID control than for PID control. Results similar to those in Fig. 8 were
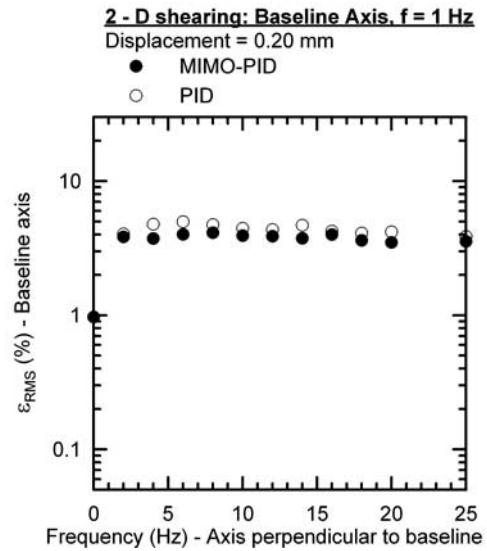

FIG. 8—*Normalized root mean square of tracking errors on baseline axis for varying frequencies of excitation on perpendicular axis (PID and MIMO-PID controllers).*

obtained when the baseline axis is rotated 90 deg (i.e., there is no significant difference in the ability of the device to control motions in the two horizontal directions). Although not shown for brevity, Fourier spectra of baseline-axis feedback signals with and without perpendicular excitation are indistinguishable (i.e., there is no permutation of the spectra at the excitation frequency for the perpendicular axis).

Broadband Command Signal Tracking

The PID and MIMO-PID controllers have the ability to command realistic earthquake waveforms in two horizontal directions, which is a unique capability of the DC-SS device. An accelerogram from the $M_w=7.6$ Chi Chi Taiwan earthquake is used to demonstrate this ability. The selected accelerogram was recorded in Wufeng, Taiwan, on firm soil (record TCU065, 90-deg component), and is digitized at a time step of 0.005 s (Nyquist frequency=100 Hz). The acceleration history is applied to the laboratory specimen as a displacement history because (1) shear stress at a particular depth in a soil deposit is proportional to average accelerations of soil above that depth, and (2) shear strains (and hence shear displacements across an element) are roughly proportional to shear stress (for an equivalent-linear shear modulus). Hence, it follows that shear deformations of a soil element would have waveforms with similar phasing to an acceleration history.

Figure 9(*a*) shows the tracking of the Taiwan displacement history for unidirectional shaking under MIMO-PID control along a baseline axis with the input scaled to produce a peak displacement of 0.2 mm. Comparison of the Fourier spectra in Fig. 9(*d*) indicates that the signal tracking is generally reasonable for frequencies less than approximately 35 Hz. At higher frequencies, the feedback signal becomes dominated by noise. During time windows with relatively large amplitude command signals (e.g., Fig. 9(*c*)), tracking errors are small. Conversely, during time windows with effectively zero command signal (Fig. 9(*b*)), the feedback signal consists of noise that is random with variable amplitude. We have investigated the amplitude of the noise feedback signal under conditions of zero command. As shown in Fig. 10, the feedback signal was found to be
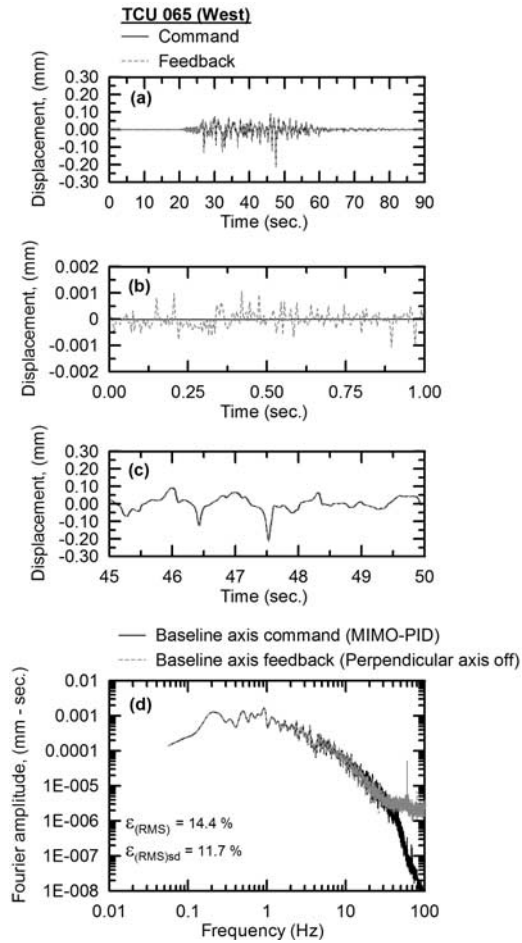
FIG. 9—*Reproduction of recorded history for shearing on one axis at a time (i.e., without interaction effects; MIMO-PID controller).*

FIG. 10—*Distribution of peak values of noise feedback signal with pump on and zero command signal along with log-normal probability distribution fit to the data.*

normally distributed with a mean value that is effectively zero and standard deviation $=0.00027$ mm. Because of these noise signals, large root mean square errors (ε_{RMS}) accumulate during time windows with low command amplitudes, such as that shown in Fig. 9(b).

Because earthquake recordings contain time windows with both weak and strong motions, the ε_{RMS} values tend to be much larger than those for sinusoidal command signals at a common peak amplitude. For example, at a peak amplitude of 0.2 mm, $\varepsilon_{RMS} \approx 14.4$ % for the Taiwan broadband command whereas $\varepsilon_{RMS} \approx 1.1$ % for harmonic command. These high ε_{RMS} values can be misleading, because it is generally the large-amplitude window of the broadband signal that is of the greatest engineering interest. Accordingly, to reduce contributions to ε_{RMS} from low-level shaking at the beginning and end of the acceleration record that may be of little engineering significance, error can be calculated using the time window during which the normalized Arias intensity increases from 5 to 95 % (the length of this time window is typically referred to as the significant duration). Root mean square errors calculated within the window of significant duration are referred to as $(\varepsilon_{RMS})_{SD}$, and are reduced from $\varepsilon_{RMS}=14.4$ % to $(\varepsilon_{RMS})_{SD} =11.7$ % for the full record (see Fig. 9(d)).

Figure 11 shows $(\varepsilon_{RMS})_{SD}$ values for the baseline axis as a function of peak displacement amplitude for cases of unidirectional shaking and multidirectional shaking (MIMO-PID and PID con-
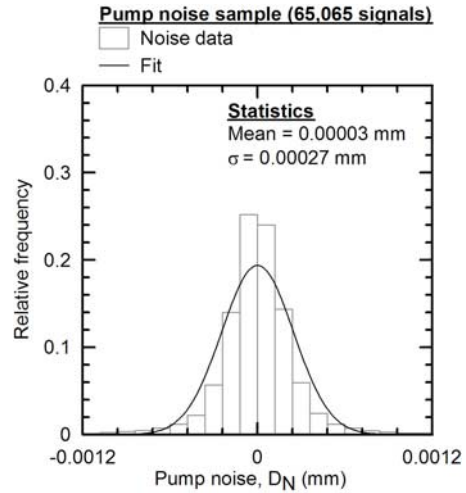
trol). For the case of multidirectional shaking, identical command signals were applied in both horizontal directions. Several important trends are illustrated by the results as follows: (1) the tracking error decreases markedly with increasing peak displacement amplitude for both unidirectional and multidirectional shaking for $u < \sim 0.2$ mm, as was the case with harmonic loading (Figs. 11(a) and 11(b)); (2) tracking errors along the baseline axis are not affected by whether the command is one-directional along that axis (e.g., MIMO-PID 1-D in Fig. 11(a)) or whether bidirectional command is used (e.g., MIMO-PID 2-D in Fig. 11(a)); (3) tracking errors for unidirectional shaking (Fig. 11(a)) and multidirectional shaking (Fig. 11(b)) are smaller for MIMO-PID control than for PID control. Although not shown for brevity, results are very similar to those in Fig. 11 when the baseline axis is rotated 90 deg.

Example Test Result for Dry Clean Sand

To illustrate the capabilities of the device in actual tests of soil specimens, we tested specimens of clean uniform sand (Silica No. 2). The sand is relatively uniformly graded with $D_{50}=1.75$ mm and has maximum and minimum void ratios of 1.02 and 0.69, respectively. The tested specimens were prepared to relative densities (D_R) of approximately 55 %. The accumulations of vertical strains (ε_v) during two unidirectional tests and one bidirectional test (all on separate specimens) are presented in Fig. 12. Each test was performed under a vertical stress of 101.3 kPa using a normally consolidated specimen. The Taiwan record used previously (TCU065) was applied at a peak shear strain amplitude of approximately 0.8 %. For the 2D test, the same record was used in both axes. The recorded feedback signals were virtually indistinguishable for all three tests, indicating repeatable controller performance. The difference between the two results for 1D shaking results from slightly different initial relative densities. The strains accumulated during bidirectional shaking are less than twice the average value of 1D shaking (i.e., average ε_v at end of 1D was 0.6 %; at end of 2D, $\varepsilon_v =0.8$ %). Note that this result differs from the multiplier of two recommended by Pyke et al. (1975).
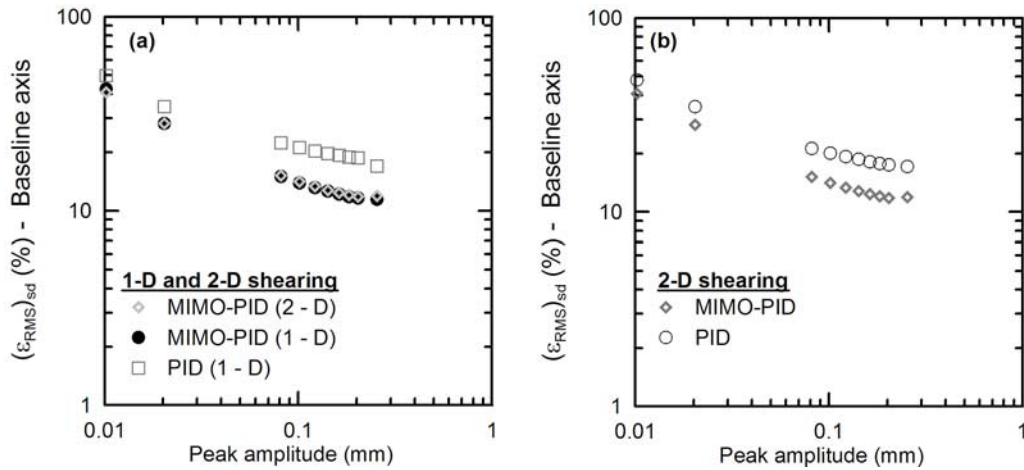
FIG. 11—*Normalized root mean square of tracking errors for unidirectional and multidirectional broadband command signals of different amplitude. Multidirectional command is with both PID and MIMO-PID control.*

Summary and Conclusions

We have described in this paper the mechanical components and control system of a state-of-the-art cyclic simple shear apparatus for soil testing. The mechanical features of this device include: (*i*) servo-hydraulic actuation to facilitate high frequency loading; (*ii*) a tri-post frame to minimize mechanical compliance effects due to rocking; (*iii*) bidirectional excitation; (*iv*) chamber pressure control for backpressure saturation; and (*v*) post-friction shear load

measurement capabilities. The device incorporates true digital control to overcome the limitations of PC-based digitally-supervised analog controllers (i.e., latency in the feedback loop and limited sophistication of control algorithms). The digital controller consists of two dSPACE DS1104 controller boards with PID and MIMO-PID control algorithms implemented at the board level. The MIMO-PID control algorithm was introduced to minimize cross-coupling effects using a LQG optimal control method and real-time system identification of feedback signals.

A series of tests were performed using harmonic command signals to characterize the performance of the device. The tracking error was quantified using normalized root mean square error (ε_{RMS}) per Eq 5 for each test. When unidirectional sinusoidal command signals were applied to each axis, the feedback signal exhibited a strong dependence of error on displacement amplitude (u) for $u < 0.2$ mm, with the smallest errors at large displacements being about 1 %. Values of ε_{RMS} were observed to increase with frequency. Cross-coupling interaction effects were found to be negligible when the device was operated with the MIMO-PID controller. Cross-coupling effects lead to larger errors when bidirectional tests were performed with the more traditional PID controller.

Uni- and multidirectional excitation was performed using a command signal adapted from a recorded earthquake motion. The command and feedback displacement histories were nearly indistinguishable for time windows with relatively large command amplitudes. However, time windows with weak command amplitudes were not well reproduced, with the feedback signal instead being dominated by noise with zero mean and standard deviation =0.00027 mm. Fourier spectra of the command and feedback signals compare favorably where the command amplitude is larger than the noise, which for the displacement history considered occurred at frequencies less than approximately 35 Hz.
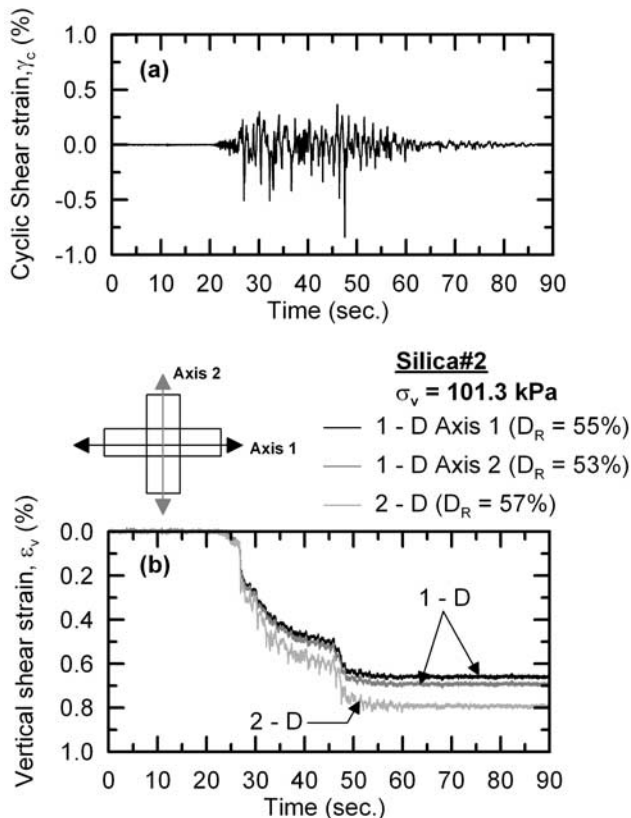

FIG. 12—*(a) Broadband displacement history applied to soil specimens in one and two horizontal directions. (b) Vertical strains experienced by separate sand specimens when displacement history from (a) is applied in single horizontal directions (denoted as 1D) and bidirectionally (denoted as 2D).*

Acknowledgments

References

Airey, D. W. and Wood, D. M., 1987, "An Evaluation of Direct Simple Shear Tests on Clay," *Geotechnique*, Vol. 37, No. 1, pp. 25–35.

Amer, M. I., Kovacs, W. D., and Aggour, M. S., 1987, "Cyclic simple shear size effects," *J. Geotech. Engrg.* 113(7), pp. 693–707.

Bhatia, S., Schwab, J., and Ishibashi, I., 1985, "Cyclic Simple Shear, Torsional Shear, and Triaxial—A Comparative Study," Advances in the Art of Testing Soils Under Cyclic Conditions, *Proceedings of a session sponsored by the Geotech. Engrg. Div., ASCE Convention*, Detroit, pp. 232–285.

Bjerrum, L. and Landva, A., 1966, "Direct Simple Shear Tests on a Norwegian Quick Clay," *Geotechnique*, Vol. 16, No. 1, pp. 1–20.

Boulanger, R. W., Chan, C. K., Seed, H. B., Seed, R. B., and Sousa, J., 1993, "A Low-compliance Bi-directional Cyclic Simple Shear Apparatus," *Geotech. Test. J.*, Vol. 16, No. 1, pp. 36–45.

Budhu, M., 1985, "Lateral Stresses Observed in Two Simple Shear Apparatus," *Soils Found.*, Vol. 27, No. 2, pp. 31–41.

Budhu, M. and Britto, A., 1987, "Numerical Analysis of Soils in Simple Shear Devices," *Soils Found.*, Vol. 27, No. 2, pp. 31–41.

Conte, J. P. and Trombetti, T. L., 2000, "Linear Dynamic Modeling of a Uni-axial Servo-hydraulic Shaking Table System," *Earthquake Eng. Struct. Dyn.*, Vol. 29, pp. 1375–1404.

DeGroot, D. J., Ladd, C. C., and Germaine, J. T., 1996, "Undrained Multidirectional Direct Simple Shear Behavior of Cohesive Soil," *J. Geotech. Engrg.*, Vol. 122, No. 2, pp. 91–98.

Doroudian, M. and Vucetic, M., 1995, "A Direct Simple Shear Device for Measuring Small-strain Behavior," *Geotech. Test. J.*, Vol. 18, No. 1, pp. 69–85.

Elgamal, A., Yang, Z., Lai, T., Kutter, B. L., and Wilson, D. W., 2005, "Dynamic Response of Saturated Sand in Laminated Centrifuge Container," *J. Geotech. Geoenviron. Eng.*, Vol. 131, No. 3, pp. 598–609.

Franklin, F. G., Powell, J. D., and Workman, L. M., 1990, *Digital Control of Dynamic Systems*, 2nd ed., Addison-Wesley, pp. 430–480.

Hazirbaba, K. and Rathje, E. M., 2004, "A Comparison Between In Situ and Laboratory Measurements of Pore Water Pressure Generation," *13th World Conference on Earthquake Engineering*, Vancouver, Canada, Paper No. 1220.

Ishihara, K. and Nagase, H., 1988, "Multi-directional Irregular Loading Tests on Sand," *Soil Dyn. Earthquake Eng.*, Vol. 7, No. 4, pp. 201–212.

Ishihara, K. and Yamazaki, F., 1980, "Cyclic Simple Shear Tests on Saturated Sand in Multi-directional Loading," *Soils Found.*, Vol. 20, No. 1.

Jafazadeh, R. and Yanagisawa, E., 1998, "Behavior of Saturated Sand Models in Multi-directional Shaking Table Tests," *Eleventh World Conference on Earthquake Engineering*, Pergamon, Elsevier, Paper No. 1049.

Kusakabe, S., Morio, S., Okabayashi, T., Fujii, T., and Hyodo, M., 1999, "Development of a Simplified Simple Shear Apparatus and its Application to Various Liquefaction Tests," *J. Geotech. Engrg.* , Vol. 617, (III/46), pp. 299–304, in Japanese.

Kutter, B. L., 1995, "Recent Advances in Centrifuge Modeling of Seismic Shaking," *3rd International Conference on Recent Advances in Geotechnical Earthquake Engineering and Soil Dynamics*, St. Louis, Missouri, Vol. 2, pp. 927–940.

Lefebvre, G. and Pfender, P., 1996, "Strain Rate and Pre-shear Effects in Cyclic Resistance of Soft Clay," *J. Geotech. Engrg.*, Vol. 122, No. 1, pp. 21–26.

Lucks, A. S., Christian, J. T., Brandow, G. E., and Hoeg, K., 1972, "Stress Conditions in NGI Simple Shear Test," *J. Soil Mech. and Found. Div.*, Vol. 98, No. 1, pp. 155–160.

Pyke, R., Seed, H. B., and Chan, C. K., 1975, "Settlement of Sands Under Multidirectional Shaking," *J. Geotech. Engrg.* , Vol. 101, No. 4, pp. 379–398.

Riemer, M. F. and Seed, R. B., 1997, "Factors Affecting Apparent Position of Steady-state Line," *J. Geotech. Engrg.* , Vol. 123, No. 3, pp. 281–288.

Saada, A. S., Fries, G., and Ker, C. C., 1982, "An Evaluation of Laboratory Testing Techniques in Soil Mechanics," *Soils Found.*, Vol. 23, No. 2, pp. 381–395.

Sheahan, T. C., Ladd, C. C., and Germaine, J. T., 1996, "Rate Dependent Undrained Shear Behavior of Saturated Clay," *J. Geotech. Engrg.*, Vol. 122, No. 2, pp. 99–108.

Shen, C. K., Sadigh, K., and Herrmann, L. R., 1978, "An Analysis of NGI Simple Shear Apparatus for Cyclic Load Testing," *Dynamic Geotechnical Testing*, ASTM STP 654, ASTM International, West Conshohocken, PA, pp. 148–162.

Tatsuoka, F., and Silver, M. L., 1981, "Undrained Stress-strain Behavior of Sand Under Irregular Loading," *Soils Found.*, Vol. 21, No. 1, pp. 51–66.

Van Overschee P. and De Moor, B.1995, "A Unifying Theorem for Three Subspace System Identification Algorithms," *Automatica*, Vol. 31, No. 12, pp. 1853–1864.

Vucetic, M. and Lacasse, S., 1982, "Specimen Size Effect in Simple Shear Test," *J. Geotech. Engrg.*, Vol. 108, No. 12, pp. 1567–1585.

Whang, D. W., Stewart, J. P., and Bray, J. D., 2004, "Effect of Compaction Conditions on the Seismic Compression of Compacted Fill Soils," *Geotech. Test. J.*, Vol. 27, No. 4, pp. 371–379.

Whang, D. H., Moyneur, M. S., Duku, P. M., and Stewart, J. P., 2005, "Seismic Compression Behavior of Non-plastic Silty Sands," *Proceedings of an International Symposium on Advanced Experimental Unsaturated Soil Mechanics*, A. Tarantino, E. Romero, and Y. J. Cui, Eds., Trento, Italy, 27–29 June, A. A. Balkema Publishers, pp. 257–263.

Wilson, D. W., Boulanger, R. W., Feng, X., Hamann, B., Jeremic, B., Kutter, B. L., Ma, K., Santamarina, C., Sprott, K. S., Velinsky, S. A., Weber, G., and Ben Yoo, S. J., 2004, "The NEES Geotechnical Centrifuge at UC Davis," *13th World Conference on Earthquake Engineering*, Vancouver, Canada, Paper No. 2497.